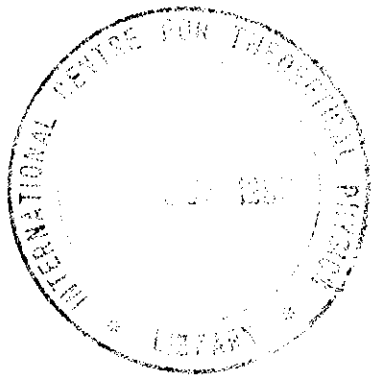

INTERNATIONAL ATOMIC ENERGY AGENCY
UNITED NATIONS EDUCATIONAL, SCIENTIFIC AND CULTURAL ORGANIZATION

INTERNATIONAL CENTRE FOR THEORETICAL PHYSICS
34100 TRIESTE (ITALY) - P.O.B. 586 - MIRAMARE - STRADA COSTIERA 11 - TELEPHONE: 2240-1
CABLE: CENTRATOM - TELEX 460392 - I

SMR/208 - 30

SPRING COLLEGE IN MATERIALS SCIENCE

ON

"METALLIC MATERIALS"

(11 May - 19 June 1987)

NEUTRON AND X-RAY SCATTERING FROM METALLIC ALLOYS, EXAFS

(Parts I and II)

C.H. DE NOVION
SESI
Centre d'Etudes Nucléaires
B.P. No. 6
92260 Fontenay-aux-Roses
France

SPRING COLLEGE IN MATERIALS SCIENCE
ON
"METALLIC MATERIALS"
(11 May - 19 June 1987)

NEUTRON AND X-RAY SCATTERING FROM
METALLIC ALLOYS, EXAFS

PARTS I and II : GENERAL ASPECTS - DIFFRACTION

C.H. de NOVION
Section d'Etude des Solides [Irradiés]
Centre d'Etudes Nucléaires
B.P. 6, F-92260 Fontenay-aux-Roses
France

INTRODUCTION

Atomic structure has been directly observed in some cases by field-ion microscopy and high-resolution transmission electron microscopy. Nevertheless:

- the precise determination of lattice constants and atomic positions in crystals,
- statistically meaningfull (for macroscopic samples) structural informations on crystalline defects,
- quantitative pair correlations in disordered systems (solid solutions, amorphous, ...),

are only obtained by a study in the reciprocal space. Indeed, <u>diffraction</u> by a perfect or imperfect crystal gives the Fourier transform of the electron (for X-rays) or nuclear (for neutrons) spatial distribution.

Historically, X-ray diffraction by crystals was discovered by Von Laue in 1912. The first neutron diffraction spectrometer was built in Argonne (USA) in 1945, and the first magnetic ordered structures were resolved in the 1950's with neutrons. Major progress was made in the 1970's, with the event of high flux neutron reactors and synchrotron radiations: this allowed in particular the development of high resolution instruments.

At the present time, considerable type of structural information can be obtained from X-ray or neutron scattering by materials. Some examples (excluding X-ray spectroscopy) are given below for crystalline solids (for amorphous systems, see the course by N.E. CUSACK):

- precise determination of crystalline structures (depending of temperature and pressure),
- thermal expansion, compressibility,
- information on bonding from electron density measurements,
- quantitative analysis of phase mixtures, phase diagrams,
- study of residual stresses, textures, grain size and morphology in polycrystals,
- kinetic studies (phase transformations, chemical reactions, ...)
- magnetic ordered structures (by neutron scattering),
- phonon dispersion curves (inelastic neutron scattering),
- strain field of point or cluster defects,
- short-range order in solid solutions or non-stoechiometric compounds, including order-disorder transitions, critical scattering, etc...
- phase separation and inhomogeneity (precipitation, cavities, ..) studies by small-angle scattering,
- mean-square atomic thermal vibration amplitudes,
- atomic diffusion (mainly hydrogen) by quasi-elastic neutron scattering.

A list of general books and review articles in the field is given in the bibliography (references [1] to [14]).

The course will contain 3 parts:

- general aspects of X-ray and neutron scattering by crystals,
- applications of (Bragg) diffraction in materials science,
- diffuse and small-angle scattering by defects.

A part n°4 will be concerned with EXAFS (Extended X-ray Absorption Fine Structure) which are the oscillations of the absorption coefficient above an edge, and inform on the local atomic structure around the absorbing atom. This technique is complementary to X-ray or neutron scattering in complex systems.

(I) GENERAL ASPECTS OF X-RAY AND NEUTRON SCATTERING BY CRYSTALS

I.1. Basis of the Kinematic theory of diffraction

Diffraction by crystals was discovered by Von Laue in 1912: when illuminating a crystal with X-rays of wavelength comparable to the interatomic distance, the X-rays were scattered in definite directions of space, leading to a regular distribution of spots on a screen.

To explain diffraction simply, consider a parallelepipedic orthorhombic crystal, with one (fixed) atom per cell, of unit translation vectors $\vec{a}$, $\vec{b}$ and $\vec{c}$, and N_x, N_y and N_z atoms in direction x, y and z. The position of an atom is $\vec{R}_{lmn} = l\vec{a} + m\vec{b} + n\vec{c}$.

The crystal is submitted to an incident beam. Source and detector are far from the crystal: the incident beam is a travelling plane wave of wave vector $\vec{k}_0$, and we look in the direction defined by the scattered wave-vector $\vec{k}$. Submitted to the incident X-ray or neutron beam, each atom is assumed to re-emit a wave of the same wavelength: the probability of scattering is low (Born approximation) and double scattering negligible. The atoms act as point sources (which is better justified for neutron scattering) with scattering amplitude b.

The phase difference between the beams scattered by atoms $\vec{R}_{lmn}$ and $\vec{R}_{000}$ (= 0) is (see figure 1):

$\vec{k} \cdot \vec{R}_{lmn} - \vec{k}_0 \cdot \vec{R}_{lmn} = \vec{Q} \cdot \vec{R}_{lmn}$. $\vec{Q} = \vec{k} - \vec{k}_0$ is the scattering vector of modulus $|\vec{Q}| = 4\pi \sin\theta/\lambda$ if 2θ is the angle between incident and scattered beam, and $|\vec{k}| = |\vec{k}_0| = 2\pi/\lambda$.

The total scattered amplitude far from the crystal (at distance R) in a direction $\vec{k}$ is then:

$$A = b \sum_{l,m,n} e^{i(-\omega t + kR + \vec{Q}\cdot\vec{R}_{lmn})} = b\, e^{i(-\omega t + kR)} \left(\sum_{l=0}^{N_x-1} e^{il\vec{Q}\cdot\vec{a}}\right)\left(\sum_{m}\right)\left(\sum_{n}\right).$$

The intensity is easily calculated to be

$$I = A^* A \propto b^2 \frac{\sin^2(Q_x N_x a/2)}{\sin^2(Q_x a/2)} \frac{\sin^2(Q_y N_y b/2)}{\sin^2(Q_y b/2)} \frac{\sin^2(Q_z N_z c/2)}{\sin^2(Q_z c/2)}$$

The function $\sin^2(Q_x N_x a/2) / \sin^2(Q_x a/2)$ is shown on figure 2: it is maximum for $Q_x a/2 = h\pi$ (h integer), its height is N_x^2, its width $2\pi/N_x$, its integrated intensity $2\pi N_x$.

Therefore, the scattering by the three-dimensional crystal occurs only in directions defined by $Q_x = h\frac{2\pi}{a}$, $Q_y = k\frac{2\pi}{b}$, $Q_z = l\frac{2\pi}{c}$, i.e. if $\vec{Q}$ is a vector of the reciprocal lattice defined by $a^* = 2\pi/a$, $b^* = 2\pi/b$, $c^* = 2\pi/c$: $\vec{Q}$ is perpendicular to the direct lattice plane of Miller indices (h, k, l). Therefore, one demonstrates easily the Bragg law:

$$|\vec{Q}| = \frac{4\pi \sin\theta}{\lambda} = 2\pi \sqrt{\frac{h^2}{a^2} + \frac{k^2}{b^2} + \frac{l^2}{c^2}} = 2\pi / d_{hkl}, \text{ or } \boxed{\lambda = 2 d_{hkl} \sin\theta}$$

(the angle of incidence and the angle of diffraction relative to plane (h,k,l) are both equal to θ, see figure 3).

If N_x, N_y and N_z are very large, the Bragg peak in the reciprocal lattice can be represented by a Dirac function, and its integrated intensity is proportional to the total number of atoms $\mathcal{N} = N_x N_y N_z$: $I_{int} \propto \mathcal{N} b^2 \sum_{hkl} \delta(\vec{Q} - \vec{\tau}_{hkl})$.

Now let us consider the diffraction by the plane $(h, 0, 0)$ and look at the width of the reflected beam in scattering angle 2θ. $I \propto \frac{\sin^2(Q_x N_x a/2)}{\sin^2(Q_x a/2)}$, the width in Q_x is $2\pi/N_x a = 2\pi/L_x$ (integral width) and differenciating $Q_x = \frac{4\pi \sin\theta}{\lambda}$, one obtains

$$\boxed{\Delta(2\theta) = \frac{\lambda}{L_{hkl} \cos\theta}}$$

This is the SCHERRER law (valid for all Bragg peaks): the width of a diffraction peak (h,k,l) is inversely proportional to the size of the diffracting domain $\perp$ to the diffracting planes.

The Bragg law shows that a monochromatic beam incident on a crystal is generally not diffracted. The condition for diffraction is that the Ewald sphere of radius $|\vec{k}| = 2\pi/\lambda$ touches a point of the reciprocal lattice (see figure 4).

This shows the origin of the three main diffracting techniques:

- Rotating crystal method: a single crystal is rotated around an axis until the Ewald sphere touches a reciprocal lattice point; by varying θ and the axis of rotation, one explores all the reciprocal space for $|\vec{Q}| \leq 4\pi/\lambda$.
- Powder method: monochromatic beam irradiating a non textured fine powder; only the small proportion of correctly oriented grains will diffract; one scans in 2θ.
- Laue method: white (polychromatic) beam, fixed θ angle for every set of planes; each of these pick the correct λ to diffract; this method is mostly used to orient single crystals.

Let us remark that there is no Bragg scattering if $\lambda \geq 2 d_{max}$, maximum interatomic distance (i.e. $2d_{100} = 2a$ for a simple cubic lattice): this is the Bragg cut-off (4.68 Å for Al).

I.2 Experimental Aspects

(a) Neutrons

Thermal neutrons from a nuclear reactor are obtained by slowing down fast neutrons by many collisions in a moderator (heavy water or graphite). One obtains a continuous Maxwellian distribution (see figure 5):

$$N(\lambda)\left(=\frac{dN}{d\lambda}\right) = \left(\frac{2N}{\lambda}\right)\left(\frac{E}{k_B T}\right)^2 e^{-E/k_B T} = \frac{c\,t_c}{\lambda^5} \exp\left(-\frac{h^2}{2 m k_B T \lambda^2}\right)$$

(m = neutron mass, E = neutron energy, h = Planck constant).

In the usual case, $T \simeq 100\,°C$, $\lambda_{max} \simeq 1$ Å, which is

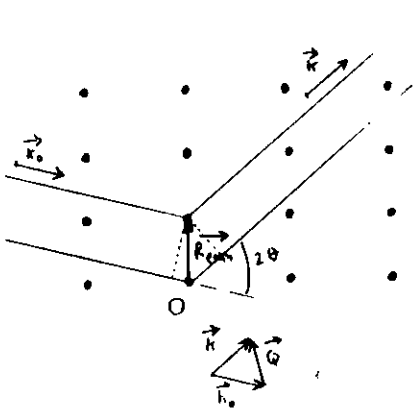

FIGURE 1

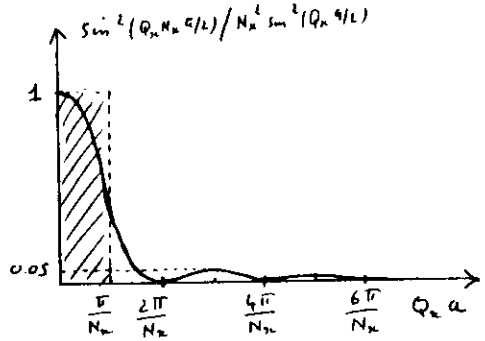

FIGURE 2

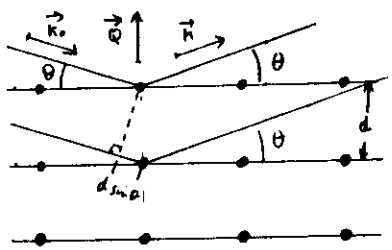

FIGURE 3 (Bragg law)

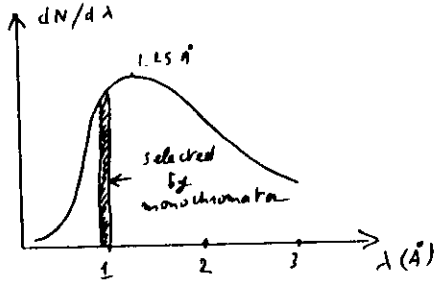

FIGURE 5 (Distribution of thermal neutrons)

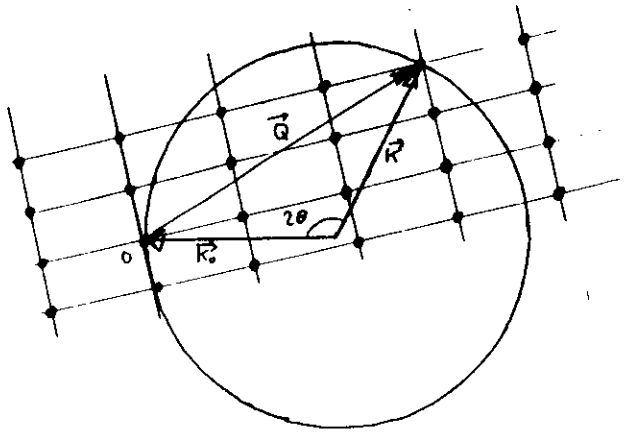

FIGURE 4
(Ewald construction)

suitable for diffraction by simple crystals. In many cases, it is interesting to have maximum flux at a smaller or larger wavelength
- small λ: allows to study far within the reciprocal space (more information for structure determination, especially liquids)
- large λ: suitable for small angle scattering, high resolution inelastic scattering

One can then use cold sources (liquid D_2, $T \simeq 20K$) or hot sources (graphite, $T \simeq 1000°C$), and work with any wavelength in the range $0.5 \leq \lambda \leq 20$ Å.

A few characteristic values ($\bar{\lambda}$: mean wavelength, $\bar{E}$: mean kinetic energy, $\bar{v}$: mean speed) are given below:

$T_{moderator}$	λ_{max} (Å)	$\bar{\lambda}$ (Å)	$\bar{E}$ (meV)	$\bar{v}$ (m/s)
400 K	0.98	1.26	51	3140
20 K	4.36	5.62	2.6	704
1300 K	0.54	0.70	167	5651

with $\bar{\lambda} = \frac{h}{\sqrt{3 m k_B T}} = \sqrt{\frac{5}{3}}\,\lambda_{max}$, $\bar{E} = \frac{3}{2} k_B T = \frac{1}{2} m \bar{v}^2$

The (relatively) low speed of neutrons will allow energy analysis by time-of-flight technique.

A typical 2-axis spectrometer (for powder or rotating-crystal diffraction or diffuse scattering), and its installation in an experimental reactor is shown on Figure 6. The neutrons are generally collimated (Soller slits) and monochromatized; the beam section is typically several cm^2, its divergency $\simeq 1°$. The monochromator allows the harmonics $\lambda/2$, $\lambda/3$, ... and these must be eliminated (for example by a graphite or beryllium filter).

A large progress was made with the use of neutron guide tubes: neutrons arriving on a surface with an incident angle

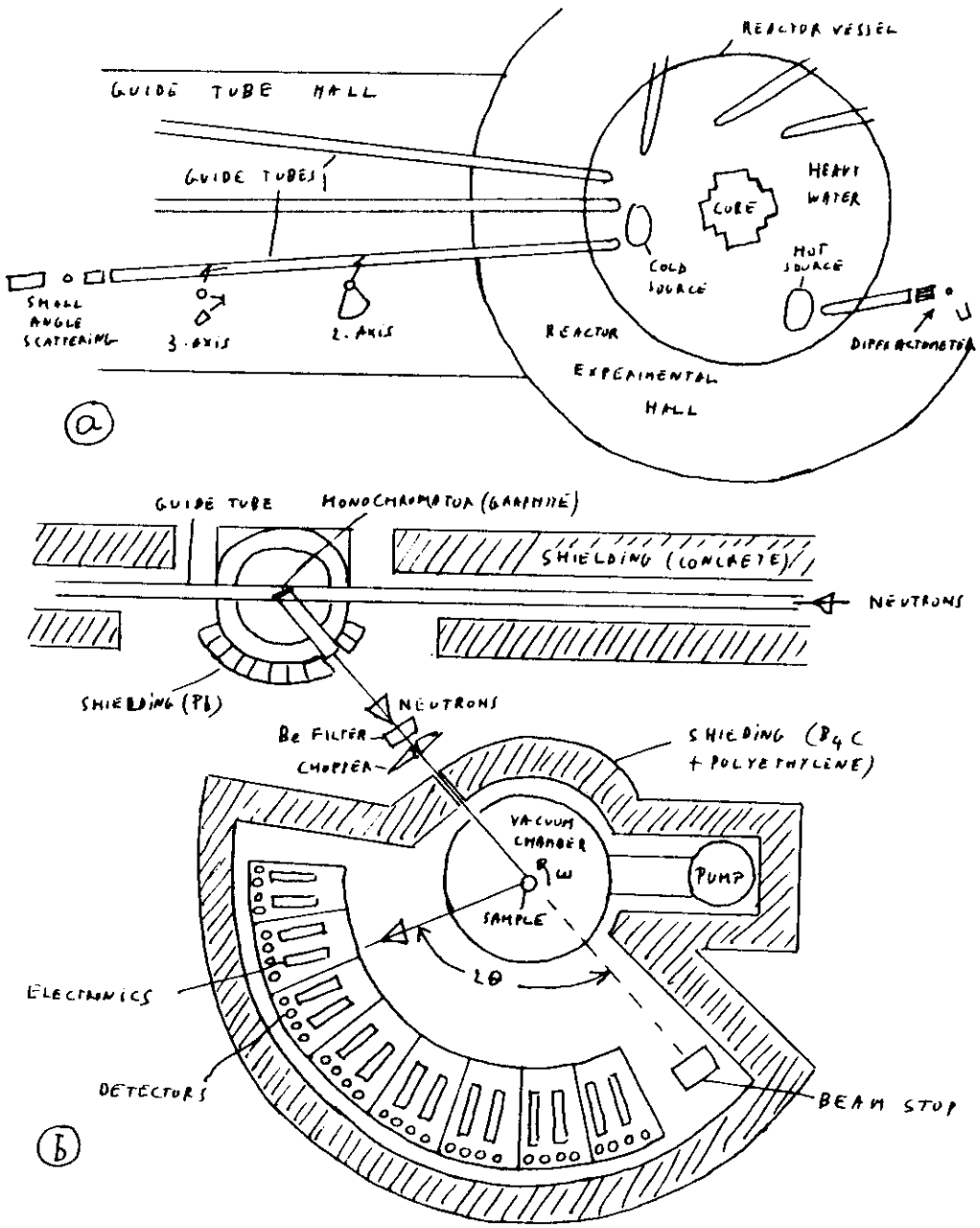

FIGURE 6 : (a) Schematic view of a high flux reactor for neutron scattering with guide tubes. (b) 2-axis spectrometer with multicounter for diffraction or diffuse scattering measurements at high temperature

smaller than the critical value $\theta_c = \lambda (N \bar{b} / \pi)^{1/2}$ ($\bar{b}$: average scattering length, N : number of nuclei per unit volume), are totally reflected ; $\theta_c = 10'$ for $\lambda = 2$ Å (for copper). Neutron guide tubes, of rectangular internal section, made of nickel deposited on glass, maintained under vacuum, and slightly curved, allow to transfer thermal or cold neutrons, without much loss, far from the reactor, in a region with very low background. Several spectrometers can be placed along a guide, each of them having a monochromator picking a different wavelength.

Typical fluxes are : 10^{15} neutrons / $cm^2 . s$ (maximum) in the reactor, $\sim 10^9$ n / $cm^2 . s$ in a guide after collimator, $\sim 10^5$ to 10^7 n / $cm^2 . s$ on the sample (after monochromator). Therefore in neutron scattering experiments, the incident flux and the statistics are low, the experiments long and expensive, and the design of an apparatus is a compromise between optimum intensity and resolution. Intensity and counting rate can be improved by large mosaic monochromators, beam under vacuum, multicounters, etc.....

Detection is by the mean of gas counters, filled by BF_3 (enriched in B^{10}) or He^3 ; each neutron produces a nuclear reaction and the charged α particles are counted. Multicounter systems, linear multidetectors (counting typically on 400 points separated by 0.2° in 2θ, i.e. $\frac{\text{x 5 mm}}{2\theta(°)}$), or square multidetectors (64 x 64 points, for small angle scattering) have been developed ; they allow to perform kinetic studies.

Energy analysis of the scattered neutrons can be made :

- by time-of-flight spectroscopy (the chopper - sample - detector distance is typically 1 to 2 m), but the signal must be pulsed and a factor 10 is again lost on the flux (Figure 7)

- or by an analyser crystal (but this is incompatible with a multidetector system).

To improve the fluxes, new are developed Spallation Sources [15] which emit pulses of neutrons; one hope that these sources could be competitive with the high flux steady state reactors for short wavelengths (hot neutrons). Diffraction spectra are then recorded by time-of-flight analysis of a white beam at fixed scattering angle.

Details on the HFR-ILL steady-state reactor (Grenoble) and on the spectrometers can be found in reference [16].

(b) X-rays

- In conventional (evacuated sealed) X-ray tubes, (see figure 8), the electrons emitted by a heated tungsten filament and repelled by a high negative voltage bombard a metal target (for example Cu, Mo, etc...). The X-ray beam is emitted by the target focus (generally of size 1 x 10 mm) and collimated in a specific direction. The X-ray spectrum consists in (see figure 9):
  - a white spectrum ("Bremsstrahlung") produced by the continuous electron deceleration in the target (λ_{min} corresponds to an X-ray energy quantum equal to the electron energy: $\lambda_{min} = 0.3$ Å for V = 40 keV),
  - characteristic lines corresponding to internal electron transitions in atoms ionized by the electrons (for example the $K\alpha_1$ and $K\alpha_2$ lines correspond to holes created in the K (1S) shell and $2P_{3/2} \rightarrow 1S$ and $2P_{1/2} \rightarrow 1S$ electron transitions respectively).

The X-rays from a target are incoherent. Most of the experiments are performed with the monochromatic characteristic lines. The K lines are very sharp ($\Delta\lambda/\lambda$ for $K\alpha_2 \sim 0.5\ 10^{-3}$). The

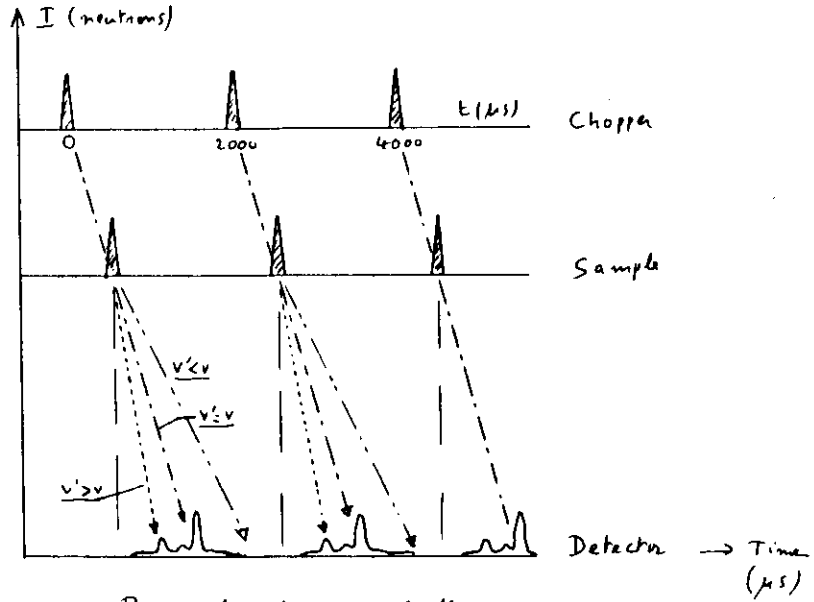

FIGURE 7: Principle of time-of-flight measurements (v: neutron velocity before sample; v': after sample).

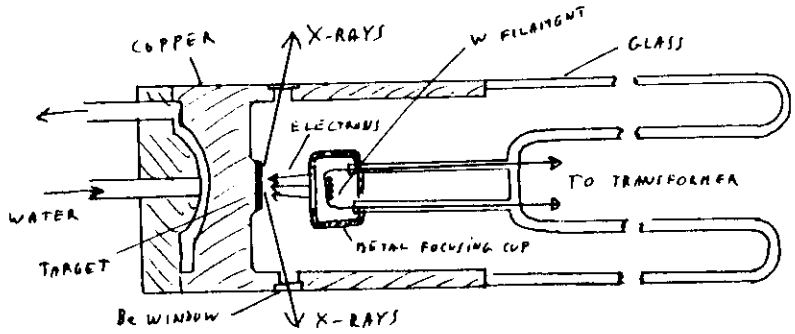

FIGURE 8: Scheme of sealed filament X-ray tube (from ref. [4])

wavelengths generally used range from 0.56 Å (22 keV, Ag target) to 2.29 Å (5.4 keV, Cr target). The flux on a sample is typically 10^9 photons/s, much larger than for neutron beams.

- In order to have larger intensities, for example for the study of point defects in low concentration by diffuse scattering, X-ray sources with rotating anodes (so that an area of the target is not always under the beam, allowing increase of intensity without excessive heating) have been developed; for example the experiment in Jülich [17] has a power of 100 kW (instead of 1 kW for a conventional tube) whence a flux of $\simeq 10^{11}$ photons/s (Cu $K\alpha$).
- Even larger fluxes ($> 10^{14}$ photons/cm^2.s on the sample) are now being obtained with synchrotron radiation [18]: the radiation emitted by the acceleration of electrons or positrons in a storage ring (with typical energies $\simeq 1$ GeV) is a white beam with wavelength ranging from $\simeq 0.5$ Å (25 keV) up to the U.V. range. The beam has a very weak vertical divergency (typically at LURE-DCI: 0.4 milliradians at 2 Å for 1.8 GeV electrons in the ring) (see <u>figure 10</u>). The beam is polarized with the electrical field vector parallel to the plane of the orbit; it is pulsed. The synchrotron radiation is now being used for the study of defects (diffuse and small angle scattering, EXAFS).
- A typical commercial X-ray diffractometer is schematized on <u>figure 11</u>. In conventional diffraction studies, the flat sample rotates by $\Delta\theta$ when the detector rotates by $\Delta 2\theta$: the sample is always in reflexion geometry, maintaining focussing.

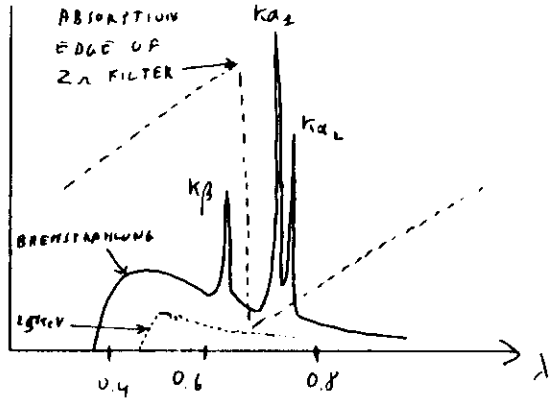

FIGURE 9: SPECTRUM OF Mo at 35 KV (from [4])

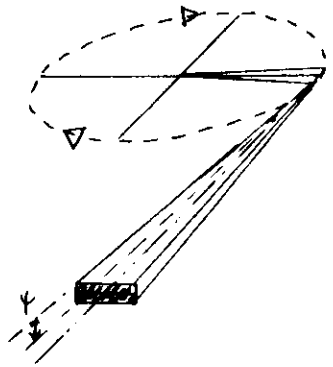

FIGURE 10: The Synchrotron X-ray beam.
(ψ vertical divergence of the beam emitted by electrons running on a horizontal circular orbit)

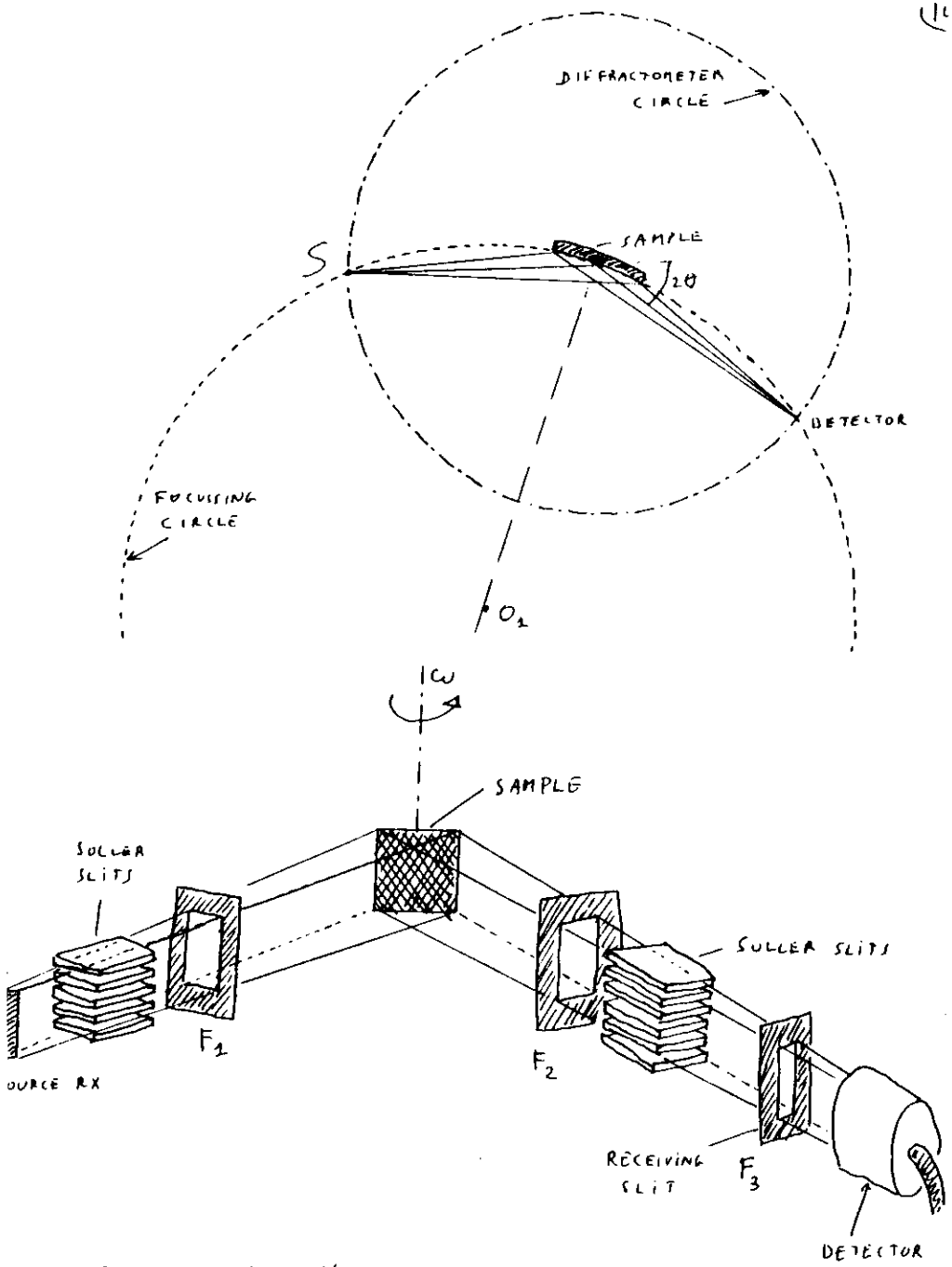

FIGURE 11 : X-RAY POWDER DIFFRACTOMETER

With conventional tubes, 3 characteristic lines are produced : $K\alpha_1$, $K\alpha_2$ and $K\beta$ of relative intensities 2, 1 and $\simeq 0.4$. A filter in the incident beam (made with the Z-1 element for a target Z, i.e. Ni filter for Cu target, the absorption edge of Z-1 being between $K\alpha$ and $K\beta$ of Z) allows to eliminate $K\beta$ and part of the Bremsstrahlung.

A monochromator on the incident beam (curved Si) can eliminate $K\beta$, $K\alpha_2$ but is very delicate to handle. A monochromator between sample and detector (curved graphite) allows to eliminate $K\beta$ and part of the fluorescence, with only small attenuation of the scattered beam. In general, people work with the doublet $K\alpha_1 - K\alpha_2$.

The main sources of systematic error on the lattice parameter a, are:
- the exact position of the effective (irradiated) centre of the specimen at the mechanical centre of the spectrometer (corrected by an extrapolation of $a = f(\sin^2\theta/\cos\theta)$ at $\theta = \pi/2$),
- the shape of the Bragg peaks : choice between peak maximum or centre of gravity, asymetry caused by the Soller slits or non-uniform intensity distribution in the beam, weight of the tails, broadening due to microstructure of the sample, etc....

Relative accuracies of $\Delta a/a \simeq 10^{-4}$ can be achieved (absolute accuracies $\simeq 10^{-3}$).

- Precise single crystal measurements are made with modern automatized 4-circle diffractometers (1 scan in 2θ and ω). Typical sample sizes are 0.1 mm^3. Monitoring beam intensity is necessary for precise intensity measurements.
- X-ray detection is made by films or counters. The latter are gas proportional counters, scintillation counters (NaI crystal activated with Tl), or solid-state (intrinsic Ge) detectors.

The solid state detectors have a few hertz resolution (3% instead of 25% for the gas counter, and even more for the scintillator), but are more expensive. These counters are linear up to 20000 - 50000 counts/s. Position sensitive linear detectors are also developed.

I.3 Interaction with matter

(a) The scattering of X-rays by atoms

X-rays are scattered by an electron by two processes:

- elastic coherent (Thomson) scattering: the electron accelerated by the electric field $\vec{E}$ of the incident X-ray beam oscillates and emits a radiation of same wavelength; taking into account the two components of $\vec{E}$ (// and $\perp$ to the scattering plane), one obtains: $I_e / I_0 = \frac{e^4}{m^2 r^2 c^4} \left(\frac{1+\cos^2 2\theta}{2} \right)$ at distance r. (e: electron charge, c: speed of light, $\frac{1+\cos^2 2\theta}{2}$: polarization factor); it is this coherent scattering which contributes to diffraction.
- inelastic incoherent (Compton) scattering: some energy of the incident photon is transferred as kinetic energy to the electron; the increase of wavelength is (in Å): $0.0243\,(1-\cos 2\theta)$, independent of λ and increasing with θ; there is no fixed relation to the incident beam phase, and the Compton scattering cannot participate to the diffraction (but it does to the background). The relative importance of Compton scattering is large for light elements (more weakly bound electrons).

If one considers an atom, each electron contributes to the Thomson scattering; in the forward direction ($\theta = 0$), there is no phase difference between the X-rays scattered by the different electrons, and the atomic scattering amplitude (relative to the single electron scattering amplitude) $f(\theta=0)$ is equal to Z (atomic number). For $\theta \neq 0$, there is a phase difference as the size of the atom is comparable to the wavelength ($\simeq 1$ Å): a similar treatment as in § I.1 gives $f(\theta) = \int \rho(\vec{x})\, e^{i \vec{Q}.\vec{x}}\, d^3\vec{x}$, where $\rho(\vec{x})$ is the atomic electron density in $\vec{x}$. $f(\vec{Q})$, Fourier transform of the atomic electron charge density, decreases with θ as shown on figure 12. (The factor $1/m^2$ in the Thomson scattering cross-section explains that the nucleus scattering is negligible).

When the incident photon energy approaches an absorption edge, the electrons associated with the absorption move out of phase; this causes a destructive interference and a reduction of f; moreover, the strong absorption just above the edge introduces an imaginary part in f; the atomic scattering factor has to be corrected and becomes $f + f' + if''$. Typically, for zinc, $f(\theta=0) = 30$; near the K edge, f' amounts to -9 and f'' to +4 (see figure 13). Scattering with λ near an edge is called anomalous scattering; it allows, using for example the white beam of a synchrotron, to separate in an alloy two elements of neighbouring Z (and f's). An example will be shown on small angle scattering.

(b) The scattering of neutrons by atom nuclei

As the neutrons carry no charge, their interaction with electrons is generally negligible (except in magnetic materials, see below). The main interaction is with the nuclei, via nuclear forces. As the size of the nuclei ($\approx 10^{-13}$ cm) is much smaller than λ, one sees that the scattering amplitude b is independent of θ (and $\vec{Q}$) (see figure 12). Contrary to the f factor for X-rays, b cannot be calculated. But is determined experimentally [2].

In fact, the nucleus scattering amplitude (or "scattering length"):
- is different for different isotopes of the same element,
- depends of the relative orientation of the nucleus and neutron spin.

One defines a coherent scattering length $\overline{b}$ which is the average scattering length taking into account the isotope concentrations, and relative spin orientation probabilities. The coherent scattering cross-section is $4\pi \overline{b}^2$ (*)
An incoherent scattering cross-section, $4\pi(\overline{b^2} - \overline{b}^2)$ comes from the randomness of the isotope distribution and relative spin orientation (in a similar way as the Laue cross-section in alloys, see § III). The total cross-section is $\sigma = \sigma_{coh} + \sigma_{inc}$ ($\simeq 1\,barn = 10^{-24}\,cm^2$).

Figure 14 compares the variation of coherent b with atomic weight, to that of f (X-rays). b can be negative (phase-shift of 180° at the scattering if one is near a resonance). Contrary to X-rays, the b values of light elements are comparable to those of heavy elements. Two neighbouring elements in the periodic table can have very different b's (when the f's are nearly equal). Isotope substitution can allow to change b and differentiate the scattering amplitudes of two elements in an alloy.

(*) The interaction between neutron and nuclei is weak and one may apply the Born approximation which states that the diffracted wave is proportional to the Fourier transform of the interacting potential (in the present case: delta function).
If the incident normalized neutron (plane) wave function is $|\psi_0\rangle = \frac{1}{\sqrt{V}} e^{ikz}$, the scattered wave function is spherical $|\psi_1\rangle = \frac{1}{\sqrt{V}} \frac{b}{r} e^{ikr}$, and the scattering cross-section is:

$$\sigma = \frac{\text{outgoing current of scattered neutrons}}{\text{incident neutron flux}} = \frac{4\pi r^2 \langle \psi_1 | v | \psi_1 \rangle}{\langle \psi_0 | v | \psi_0 \rangle} = 4\pi \overline{b}^2,$$

and the differential cross-section (isotropic in the present case) is $d\sigma/d\Omega = \overline{b}^2$ (v = neutron velocity, V = volume).

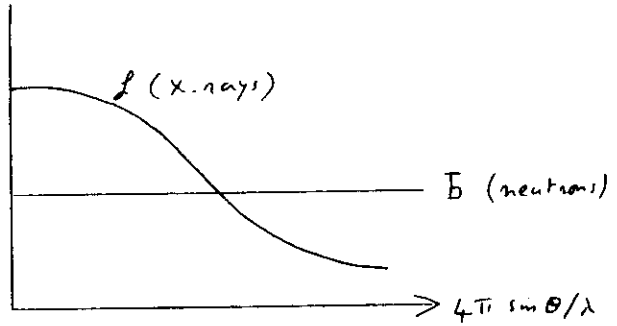

FIGURE 12

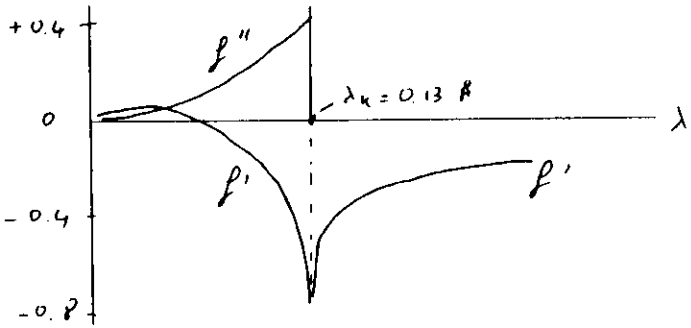

FIGURE 13 : Anomalous dispersion corrections (schematic - K-edge of Zn).

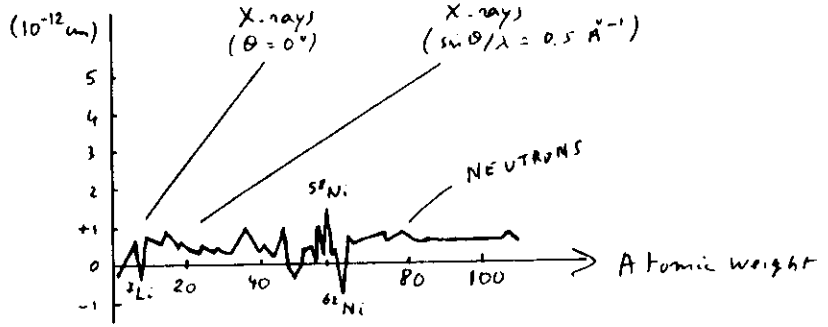

FIGURE 14 : Neutron and X-ray scattering amplitudes versus atomic weight (from ref. [2]).

For example:
- for nickel $b(^{58}Ni) = 1.44\ 10^{-12}$ cm, $b(^{60}Ni) = 0.30\ 10^{-12}$ cm, $b(^{62}Ni) = -0.87\ 10^{-12}$ cm;
- vanadium has an extremely small coherent cross-section ($b = -0.05\ 10^{-12}$ cm, $4\pi b^2 = 0.03$ barns) and a large incoherent cross-section (5.1 barns);
- hydrogen has a very large incoherent cross-section (81.5 barns, compared to $4\pi b^2 = 1.76$ barns).

It is only the coherent scattering amplitude b which contributes to Bragg diffraction. Incoherent scattering gives a constant background in the diffraction patterns. Hydrogen (and impurities) are therefore to avoid impatively.

ⓒ The magnetic scattering of neutrons

There is an interaction of the neutron spin with the magnetic moment of an atom (in most metals and alloys, which are weak Pauli paramagnets, this is negligible). The scattering cross-section $d\sigma/d\Omega)_m$ of neutrons by an ion of spin S is $\frac{2}{3} S(S+1) \left(\frac{e^2 \gamma}{mc^2}\right)^2 f_m^2$ (paramagnetic scattering), where f_m, magnetic form factor, is the Fourier transform of the electron density for an electron $(\int 4\pi r^2 \rho(r) dr = 1)$ in the incomplete shell responsible of magnetism. f_m therefore varies with θ similarly to the X-ray atomic scattering amplitude. Both are function of $|\vec{Q}| = 4\pi \sin\theta / \lambda$.
(γ magnetic moment of the neutron in nuclear magnetons).
For Mn^{2+}, $d\sigma/d\Omega)_m = 1.69$ barns ($S = 5/2$).

ⓓ Structure factors

In the case of neutron scattering, where the scattering nuclei can be assimilated to points, the extension of the results of § I.1 is straightforward.

For an assembly of fixed atoms α, the scattering amplitude at large distance is $\mathcal{A} = \sum_\alpha b_\alpha e^{i\vec{Q}\cdot\vec{R_\alpha}}$. For a small perfect crystal, where the position of the cell is $\vec{R_{lmn}}$ and that of an atom in the cell $\vec{r_j}$ (relative to $\vec{R_{lmn}}$),

$$\mathcal{A} = \sum_{lmn} e^{i\vec{Q}\cdot\vec{R_{lmn}}} \sum_j b_j e^{i\vec{Q}\cdot\vec{r_j}}.$$

The quantity $F(\vec{Q}) = \sum_j b_j e^{i\vec{Q}\cdot\vec{r_j}}$ is called the structure factor of the crystal. One has $\mathcal{A} = F(\vec{Q}) \sum_{lmn} e^{i\vec{Q}\cdot\vec{R_{lmn}}}$, and the scattered intensity is $I \propto \frac{d\sigma}{d\Omega} \propto |F(\vec{Q})|^2\ \delta(\vec{Q} - \vec{\tau_{hkl}})$, pondered sum of delta functions centered on the reciprocal lattice points $\vec{\tau_{hkl}}$.

For a crystal with one atom per cell, $F_{hkl} = b$, $\forall\ h, k, l$.
For a body-centered cubic metal, $F_{hkl} = 0$ if $h+k+l$ is odd, because the two atoms in the cell, 000 and $\frac{1}{2}\frac{1}{2}\frac{1}{2}$, scatter then out of phase: $F = 1 + e^{i\frac{a}{2}\left(h\frac{2\pi}{a} + k\frac{2\pi}{a} + l\frac{2\pi}{a}\right)} = 1 + e^{i\pi(h+k+l)} = 0$
(for $h+k+l$ even, $F = 2$)

For the f.c.c. rocksalt structure NaCl, $F \neq 0$ only if $h+k$, $k+l$ and $l+h$ are even, with $F = b_{Na} - b_{Cl}$ if $h+k+l$ is odd and $F = b_{Na} + b_{Cl}$ if $h+k+l$ is even.

In the case of X-ray scattering, one uses generally the same formula as for neutrons, the b being replaced by the atomic factors f. This is of course not exact, as the valence electron spatial distribution is changed relatively to that of neutral atoms. $F(\vec{Q})$ must be taken as the Fourier transform of the electron charge density in the elementary cell.
The measurement of integrated diffracted intensities allows to determine the $|F|^2$ and by least squares method to solve crystal structures.

ⓔ Thermal vibrations

They have several consequences:

- they modify slightly the spatial distribution of the charge density, especially for light elements (one may have interest to couple neutron and X-ray diffraction which inform respectively on the nuclei and on the electronic cloud distribution);
- they attenuate the atomic scattering amplitudes (without broadening of the Bragg peaks, at 3 dimensions), by the Debye-Waller factor: f_j becomes $f_j \exp\left(-\frac{8\pi^2}{3}\langle u_j^2\rangle \frac{\sin^2\theta}{\lambda^2}\right)$ for isotropic vibrations of mean square amplitude $\langle u_j^2\rangle$. (Static displacements, due for example to the size effects in a solid solution, give a somewhat similar attenuation, see § II);
- inelastic scattering (called also "thermal diffuse scattering") due to absorption or emission of phonons by the incident particle; this gives small tails to the Bragg peaks, and has to be corrected (by calculation) in high precision diffraction measurements, especially at high temperature. It is generally a small correction at room temperature ($\sim 1\%$).

Inelastic scattering of neutrons by single crystals allows to determine the phonon dispersion curves (and also the spin wave dispersion curves in magnetic crystals). The measurements are usually performed with a 3- (vertical) axis spectrometer (figure 15). The scattering obeys to the conservation laws:

$$\begin{cases} \hbar(\vec{k} - \vec{k}_0) = \hbar\vec{Q} = \hbar(\vec{q}_{ph} + \vec{\tau}) \\ \frac{\hbar^2}{2M}(k_0^2 - k^2) = \pm\hbar\omega_{ph} \end{cases}$$

, where $\vec{\tau}$ is a reciprocal lattice vector,

(+ for phonon creation, - for phonon annihilation)

ω_{ph} = phonon frequency, $\vec{q}_{ph}$ = phonon wavevector in the first Brillouin zone.

The sample is set with the reciprocal lattice plane to study horizontal. One wants for example to scan in ω

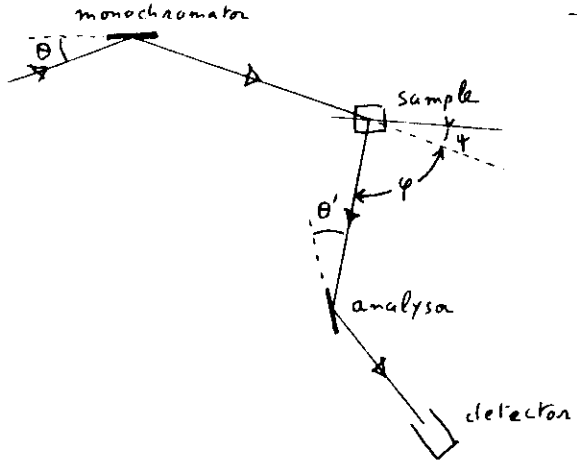

FIGURE 15

3 axis neutron spectrometer. Determination of phonon dispersion curves by the constant $\vec{Q}$ scans.

Example: curves $\omega(K)$ obtained on b.c.c. Zn-β at 1150°C by STASSIS et al (Phys. Rev. Lett. 41, 1726 (1978)).

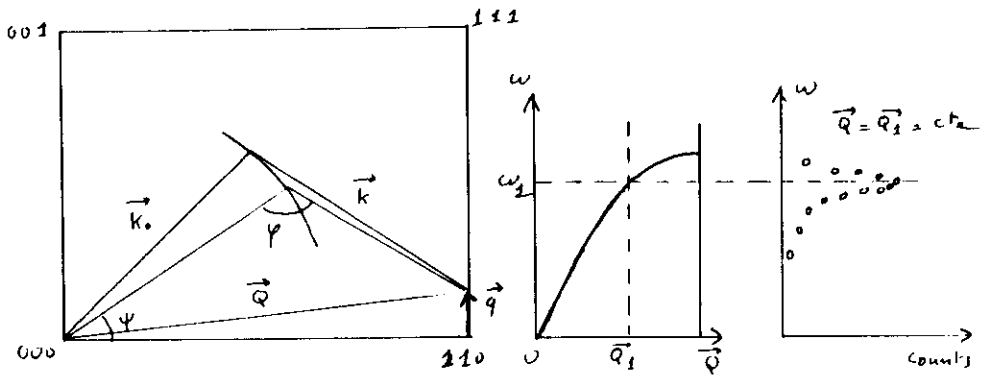

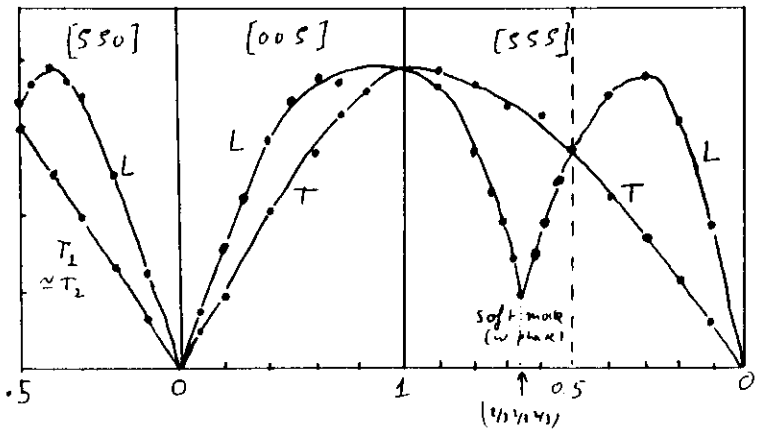

Zn β

T = 1150°C

for a given $\vec{Q}$, with a given incident wavevector $\vec{k_0}$. This is done by varying φ (scattering angle) and ψ (orientation of the crystal relative to the incident beam).

① Absorption, extinction, etc.....

They are major parameters in X-ray or neutron scattering.

- Neutron true absorption occurs by nuclear reactions; for most of the elements, this is weak and the linear absorption coefficient μ is of the order of 0.1 to 1 cm^{-1} (see table of values in [2]). μ increases linearly with the wavelength. Many elements are extremely transparent to thermal neutrons (C, Al, Fe, Zn, NS, ...). There are a few cases where the absorption, due to a resonance between the incident neutron and the internal energy structure of the nucleus, is very large: B^{10}, Cd^{113}, Sm^{149}, Gd, Eu. Materials containing these elements (i.e. B_4C, Cd, ..) are used to collimate the beam and included in the shielding (biological, and to decrease background).
  The experimental intensities must be corrected for total absorption (true absorption + absorption due to scattering).

- X-ray absorption is much larger; it is mostly due to electron transitions within the atoms. For a given branch of the absorption curve (between two definite edges), it varies as $\lambda^3 Z^3$. absorption is maximum for heavy elements and long wavelength. For metals, at $\lambda = 1.54$ Å, μ varies typically between 2.7 cm^{-1} (Be, used for windows) to 1311 cm^{-1} (Al) and 26310 cm^{-1} (Pb). Therefore, the thickness sampled by X-rays varies from $\simeq 0.1$ mm for Al to less than 10 µm for Pb.

- Extinction plays an important role in the study of (nearly) perfect crystals.

Primary extinction is due to the attenuation of the incident beam by the successive Bragg reflexions on a whole set of parallel (h k ℓ) planes. As the reflexion power is typically 10^{-4}, thickness of 1000 Å ($\simeq$ 500 planes) attenuates the beam by $\simeq 5\%$ (in fact primary extinction is more complex, and interference of double-scattered beam with the incident beam plays a role). Therefore perfect domains of size > 0.1 µm will distort the intensities appreciably and decrease the strong reflexions compared to the weak. Hopefully, all crystals contain dislocations which divide them into slightly disoriented ($\simeq 0.1°$) mosaic blocks ("ideally imperfect crystals"); these blocks will diffract at slightly different angles. Mosaicity decreases the extinction and allows larger penetration of the incident beam; but one may still have secondary extinction due to the encounter of several mosaic blocks with the same orientation; it can be corrected to a certain degree by measurements at different wavelengths.

Comments on incoherency (or independent scattering): if two diffracting sources are far apart, i.e. 1 µm, then interference will oscillate at least 10 times within the resolution of a diffractometer ($\Delta\theta \simeq 10^{-3}$ radians) and will be averaged; one will measure the sum of then scattered intensities (not amplitudes). The same occurs with slight random phase distribution such as that due to mosaicity. Therefore, one can define a coherence length for X-ray or neutron scattering in materials, which is generally in the range 10^3 - 10^4 Å. One understands then that for a 2-phase specimen, it is the scattered intensities, not the amplitudes, which are additive.

- Multiple Bragg scattering has to be corrected in large samples.
- In polycrystal studies, care should be taken with texture.

I. 4 Comparison of neutrons and X-rays

X-ray scattering has been up to now much more used than neutron scattering. It offers indeed several decisive advantages:

- X-rays are much cheaper; every laboratory can have a good classical diffractometer,
- the available fluxes are much larger, even with commercial classical tubes ($factor > 10^3$ compared to neutrons); this allows short experiments ($\simeq$ 1 hour for powder diffraction) and small specimens (neutrons require generally large samples),
- as a consequence of the large available intensities, and of the sharpness of characteristic reflections, one can have very high resolution (in θ and $\vec{Q}$) apparatus: this is for example needed for Huang scattering (see § III) which is always performed with X-rays, not neutrons; the lattice parameter determinations are more precise, and multiphase diffraction spectra more easily analysed;
- it allows to study lower defect concentrations (10^{-4} in diffuse scattering [17], instead of 10^{-3} with neutrons in the best conditions);
- one can study gradients of composition or strain (typically by slices of 0.01 mm).

Nevertheless, neutrons present specific advantages:

- they allow to study light atoms (C, N, O, ...), or to differentiate neighbouring elements of the periodic table (Cu_{29}, Ni_{28});
- they are much better adapted to high temperature studies, as one can measure on a bulk sample in a sealed container, avoiding oxidation or composition changes by evaporation, and as the furnace is transparent to neutrons;
- one can study magnetic ordered structures, phonon (or magnon) dispersion curves, ...

- the use of isotopic substitution can be interesting, either to determine pair correlations in multicomponent amorphous or disordered systems, or to eliminate simple or multiple Bragg scattering in polycrystals ("null matrix" with $\overline{b} = 0$, see § III);
- the (quasi-) independance of b versus $\sin\theta/\lambda$ is an advantage;
- measurements are representative of bulk sample ($\simeq 1\ cm^3$), (but gradients cannot be studied);
- inelastic scattering can be separated experimentally, by time-of-flight techniques or analyser crystal; this cannot be done with X-rays.

Considering diffracted intensity statistics, the low neutron absorption (which reduces by a factor $\simeq 100$ the advantage of X-rays), and the use of multidetectors allows to perform a powder neutron diffraction experiment in a time comparable to that with classical X-ray diffractometers; kinetic studies can be now performed at the minute time scale. Of course the predicted development of synchrotron radiation will give enormous advantage to X-rays.

At last, one must remember that X-ray and neutron scattering measurements are bulk measurements, and that local information at the μm range or less can only be obtained by techniques such as electron microscopy.

(II) APPLICATIONS OF BRAGG DIFFRACTION IN MATERIALS SCIENCE

II.1. General scope

In metallurgical studies of alloys, three main types of information are obtained from diffraction experiments:

- the positions
- the profiles
- the intensities

} of diffraction lines or spots

Many experiments are performed on polycrystalline samples, and this can give already a lot of information. Moreover, there are specific interests in polycrystals: textures, internal stresses, small particles, etc....

We shall not detail here the practically important studies of polyphase samples and phase detection. Of great help is the card system kept up by the Joint Committee on Powder Diffraction Standards, with the d spacing of the strongest peaks of more than 26 000 substances [search programs are available]. Let us also mention the recent importance, in the case of neutron powder scattering (in particular when many reflexions overlap) of the "profile refinement" technique developed by Rietveld [19]. Typically, conventional diffraction cannot detect less than 2-3% of precipitate, whence the importance of selected chemical dissolution and extraction methods.

(a) Positions of the lines

The study of the positions of the lines versus temperature or pressure allows to obtained respectively the thermal expansion and the compressibility.

At constant T and P, a change of position of the line for a solid solution is generally due to a change of lattice parameter (i.e. of composition, cf. Vegard's law): this allows to determine phase limits in the phase diagram. Measurement of lattice parameter is often used in a two-element solid solution as a determination of composition.

Let us mention a few experiments which need to perform lattice parameter measurements in extreme conditions:

- an example of X-ray high-pressure measurements (compressibility and phase transformations of Eu and Cs up to 27 GPa) is given in ref. [20];
- the precipitation of titanium and chromium carbides in 20% strained austenitic stainless steels containing 0.4% Ti and 0.05% C (weight), during 24 hours isochronal anneals around 700°C results in a decrease of the lattice parameter by $\simeq 10^{-3}$ Å [21];
- the change of lattice parameter due to introduction of point defects ($\simeq 10^{-4}$ Frankel pairs) by irradiation and the subsequent recovery by thermal annealing for several materials;
- the measurement of lattice parameter near the melting point of metals, combined to length measurements, for the determination of equilibrium vacancy concentration [22] (see below).

In general, lattice parameter measurements are more precise with X-rays than with neutrons, because of the narrower linewidth (although the instrumental profile with conventional neutron spectrometers is very nearly gaussian, while the X-ray profile is more complex).

Peak shifts in diffraction spectra can also be due to internal stresses (see below).

(b) Line profiles

Line broadening (compared to the experimental width) occurs in several cases, in particular:

- if the diffracting particles are small (Scherrer law, § I.1),
- if the sample is submitted to inhomogeneous strains,

- in case of composition gradients in a solid solution (which lead to a variation of lattice parameter from point to point),
- if the sample contains stacking faults.

The small size of diffracting particles can be due to fine powders, precipitates in a matrix, small mosaic blocks, dislocations, small ordered domains in a disordered matrix, etc....

When broadening is only due to particle size and strains, the two effects can be separated by a Fourier analysis of the peak shape, after deconvolution by the instrumental line shape [14]. The study must be made on at least two orders of the same diffracting plane; if we consider for example the (00 ℓ) set of a cubic crystal of lattice parameter $\underline{a}$ (i.e.: 002, 004, ...), one will have for the Bragg reflexion profile:

$$P(2\theta) = K(\theta) \sum_{n}^{\infty} \left(A_n \cos\left[2\pi n (h_3 - \ell)\right] + B_n \sin\left[2\pi n (h_3 - \ell)\right] \right), \quad (h_3 = 2a\sin\theta/\lambda)$$

where $K(\theta)$ is a slowly varying function of θ, and h_3 a continuous coordinate in the reciprocal space $\perp$ to the diffracting planes.

Generally, the peaks are symmetric, and the B_n contribute only to the long-range strains (> coherent diffraction particle size), i.e. to a change of lattice parameter.

We define ε_n as the strain in a column of length na perpendicular to the diffracting plane.

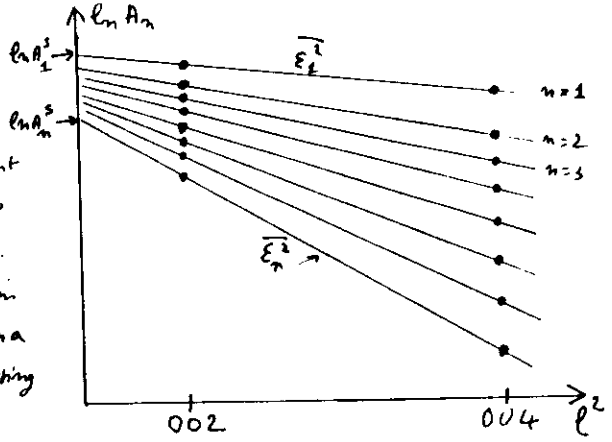

At small n, or if the distribution of ε_n is gaussian, one has:

$\ln A_n \simeq \ln A_n^S - 2\pi^2 \langle \varepsilon_n^2 \rangle n^2 \ell^2$, where $A_n^S \simeq 1 - \frac{|n|a}{L_{hkl}}$ at small n is a particle size coefficient.

The plot of $\ln A_n$ versus ℓ^2 for each n gives the mean square average strains $\langle \varepsilon_n^2 \rangle$ (see figure), and the plot of A_n^S versus $|n|$ the coherent particle size L_{hkl} perpendicular to the (h k l) planes.

The determination of strains or particle sizes requires a broadening of at least 20% of the instrumental profile; the precision on particle size (in the range 100 – 1000 Å) and strains is typically 10%. ($\left(\overline{\varepsilon_n^2}\right)^{1/2} \simeq 10^{-2}$ to 10^{-3})

A great difficulty comes from a precise determination of the background and evaluation of the tails of the peak; for example, in thin films, one has broad overlapping reflexions; simplified models have been developed taking into account the fact that the ε_n are not independent [23].

The study of line shape has also been used to obtain compositions profiles (in the $1-10^2$ µm range) and diffusion coefficients, for example in problems involving films (≃ µm thickness) deposited on metal substrates (preferably single crystals) and subsequent thermal treatments. Quantitative interpretation requires the absence of strains or small diffracting particle effects (see review by Houska [24]).

ⓒ Intensities of the lines

Let us recall, as an example, the general formula for integrated Bragg intensities by a sample without texture of volume V (neutron diffraction, powder, cylindrical specimen entirely in the parallel incident beam):

$$I_{hkl} = (\text{Cte} \times \lambda^3)\, V \frac{\rho'}{\rho} \frac{1}{\sin\theta \sin 2\theta}\, j\, N_c^2\, F_{hkl}^2\, e^{-2W}\, A_{hkl}$$

(wavelength; Lorentz; multiplicity; Debye-Waller; absorption)

(ρ = theoretical density, ρ' = true density, N_c = number of cells per unit volume, j = multiplicity of h k l diffracting planes).

Here, one has assumed the same Debye-Waller factor for all atoms.

- The integrated intensity measurements allow to obtain the structure factors $|F_{hkl}|^2$ and to determine the atomic positions in the cell. In alloys, one must consider the average occupation on each site position (average made on the coherent diffracting volume). For example:

  in disordered Cu_3Au alloys: $\bar{f} = 0.75\, f_{Cu} + 0.25\, f_{Au}$ and

  $|F_{hkl}| = 3 f_{Cu} + f_{Au}$ if $h+k$, $k+l$, $l+h$ are even, 0 unless,

  in perfectly ordered Cu_3Au: $f = f_{Au}$ on (000) sites, f_{Cu} on $(\frac{1}{2}\frac{1}{2}0)$ sites,

  $|F_{hkl}| = 3 f_{Cu} + f_{Au}$ if $h+k$, $k+l$, $l+h$ are even, $|f_{Au} - f_{Cu}|$ unless.

  But in fact, the long-range order parameter S is always smaller than 1, especially near a 2nd order disorder transition (Cu_3Au) and there are antisite atoms (Cu in the 2a sublattice and vice-versa): the superlattice reflexions are affected by this partial disorder:

  $I_{superlattice} = I(S=1) \times S^2$ (see below)

- Refinement of the diffraction spectra allows to obtain the Debye-Waller factors W_i on each site, from which one can determine the vibration amplitudes $\langle u_i^2 \rangle$. Measurements on single crystals have allowed to obtain anisotropic Debye-Waller factors.

  In alloys or non stoichiometric compounds, the measured Debye-Waller factors contain in fact a dynamic and a static contribution. If the displacements are weak, Krivoglaz [6] has shown that the static and dynamic Debye-Waller factors are additive:

  $W = W_{stat} + W_{therm}$, $W^i_{therm} = \frac{8\pi^2}{3} \langle u^2_{i,therm} \rangle \frac{\sin^2\theta}{\lambda^2}$,

  and $W^i_{stat} \simeq x(1-x) \sum_s (1 - \cos \vec{Q}.\vec{u}_s)$ in a substitutional alloy $A_{1-x}B_x$; the summation is made over all lattice sites s around a B atom; W^i_{stat} is proportional to Q^2 only at small Q. Measurements versus temperature and composition allow to separate the static and thermal mean-square displacements (see below).

(d) Magnetically ordered structures (neutron diffraction)

(For a review see IZYUMOV and OZEROV [25]).

Let us take the simple case of collinear magnetic structures (simple ferro- or antiferromagnetic) with (spin) magnetic moments in fixed orientation. The atomic magnetic differential cross-section (see § I.3.c) becomes:

$$d\sigma/d\Omega)_m = |\vec{q}_m|^2 S^2 \left(\frac{e^2\gamma}{mc^2}\right)^2 f_m^2 \qquad (f_m \text{ magnetic form factor})$$

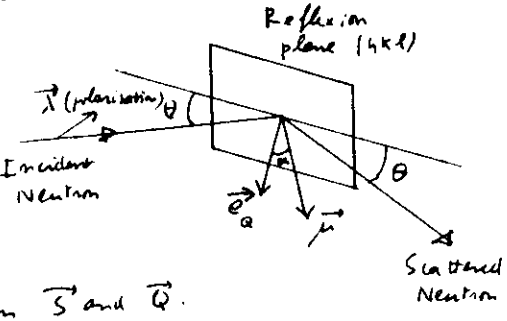

$\vec{q}_m$ is the magnetic interaction vector:

$\vec{q}_m = \vec{e}_Q (\vec{e}_Q . \vec{\mu}) - \vec{\mu}$

$\vec{e}_Q$ unit vector // $\vec{Q}$ ($\perp$ (hkl) plane)

$\vec{\mu}$ unit vector // spin $\vec{S}$

$|\vec{q}_m| = \sin\alpha$, α angle between $\vec{S}$ and $\vec{Q}$.

One defines p = magnetic scattering length $= \frac{e^2\gamma}{mc^2} S f_m = 0.54\, S f_m \times 10^{-12}$ cm

- If the neutron beam is polarized (this can be obtained by reflecting it on a ferromagnetic monochromator), i.e. all neutron spins aligned // $\vec{\lambda}$ (unit vector):

  $d\sigma/d\Omega)_{total} \sim b^2 + 2bp\, \vec{\lambda}.\vec{q}_m + p^2 q^2$

- If the neutron beam is unpolarized, the middle term in the expression above is averaged to zero and the total differential cross-section becomes $d\sigma/d\Omega)_{total} = b^2 + p^2 q^2$ (magnetic and nuclear intensities add).

In an ordered magnetic phase, if the magnetic moments scatter the neutrons in phase, one will obtain magnetic Bragg scattering.

- Ferromagnetic substances: the unit cell remains unchanged,

no new Bragg peaks, but change of the observed intensities (except if $\vec{Q} // \vec{S}$: then the magnetic scattering is zero).

- Antiferromagnetic structure : new (magnetic) unit cell and appearance of superlattice magnetic Bragg reflexions). One defines a magnetic structure factor $\vec{F}_{magn}$ summed over all magnetic atoms in the magnetic unit cell :

$$\vec{F}^{magn}_{hkl} = \sum_j \vec{q}^{\,i}_m \, p_j \, e^{\,i \vec{Q}.\vec{r}_j}$$

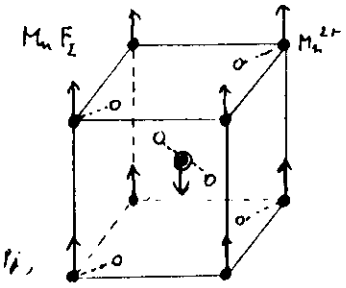

For example, in a b.c.c. antiferromagnetic in accordance with moments // <001>, the nuclear (001) reflexion is zero.

$\vec{F}^{magn}_{001} = 0$, $\vec{F}^{magn}_{100} = \vec{\mu} p_j + (-\vec{\mu}) p_j (-1) = 2\vec{\mu} p_j$,

$|F^{magn}_{100}|^2 = |F^{magn}_{010}|^2 = 4 p_j^2$: magnetic superstructure reflexion in (100), [(010) but not (001)]

On the contrary, $\vec{F}^{magn}_{200} = 0$ and the (200) nuclear intensity remains unchanged.

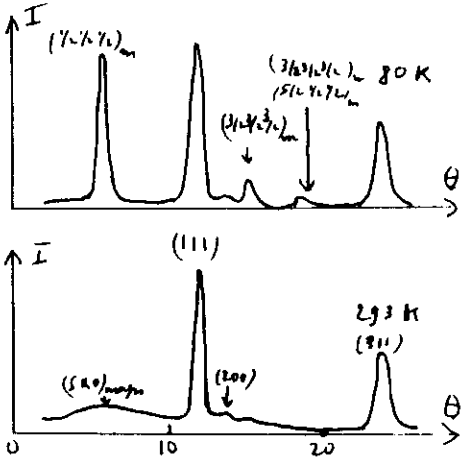

Mn O (T_N = 120 K)

(from ref [2])

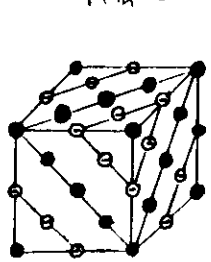

● = ↑ ○ = ↓

Moments in (111) sheets

Antiferromagnetism doubles the unit cell.

II. 2 Specific examples

ⓐ Determination of the thermal vacancy concentration by high temperature lattice parameter and length measurements [22]

Consider a crystal of N_0 atoms of atomic volume Ω_0; total volume $V_0 = N_0 \Omega_0$. An increase of T will induce :

- thermal expansion (anharmonic effects),
- thermally created point defects, which change V, N and the average Ω (because to create a vacancy one puts an atom at the surface, to create an interstitial one takes an atom from the surface) : $\frac{\Delta V}{V_0} = \frac{\Delta N}{N_0} + \frac{\Delta \Omega}{\Omega_0} + \frac{\Delta N . \Delta \Omega}{N_0 \Omega_0}$

The relative change of number of sites, $\Delta N / N_0$, will be equal to the concentration difference between vacancies and interstitials : $\frac{\Delta N}{N_0} = C_v - C_i = \frac{\Delta V / V_0 - \Delta \Omega / \Omega_0}{1 + \Delta \Omega / \Omega_0} \simeq 3 \left(\frac{\Delta l}{l_0} - \frac{\Delta a}{a_0} \right)$

for a cubic crystal of length l and lattice parameter a.

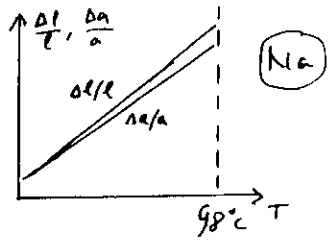

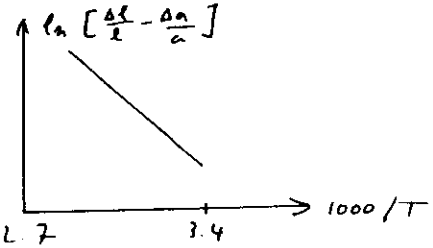

One measures $\Delta l / l > \Delta a / a \Rightarrow C_v > C_i$.

It is generally assumed that the interstitial concentration is negligible because its formation energy is $\simeq 5$ eV.

For Al, the $\ln \left[\frac{\Delta l}{l} - \frac{\Delta a}{a} \right]$ versus $1/T$ plot gives $E_v^F = 0.71 \pm 0.04$ eV, compared to 0.66 ± 0.04 from positron annihilation (role of divacancies); at the melting point, $C_v \simeq$ a few 10^{-4}.

The technique is now being developed with neutron diffraction for refractory metals (problems of windows, temperature gradient, with X-rays) [26].

(b) Superstructure reflexions and high temperature neutron diffraction

The superstructure reflexion intensity is proportional to S^2, S = long-range order parameter. One can measure $S = f(T)$ and the critical coefficient β for $(T_c - T)/T_c$ if the transition is second order. ($S \propto (T_c - T)^\beta$).

It is very difficult to detect a small 1st order transition from an apparently 2nd order, because one can have small broadening by inhomogeneities, temperature gradients, small 2-phase (ordered + disordered) region, ...

The best known (and perhaps unique) example of 2nd order transition in a 3-dimensional solid for atomic ordering, is that of Cu_2MnAl. The critical coefficient β could be determined with precision from neutron scattering [27] : $\beta = 0.293$, in agreement with the nearest-neighbour 3-dimensional Ising model (mean-field value: 0.5, rigid Ising : 0.31).

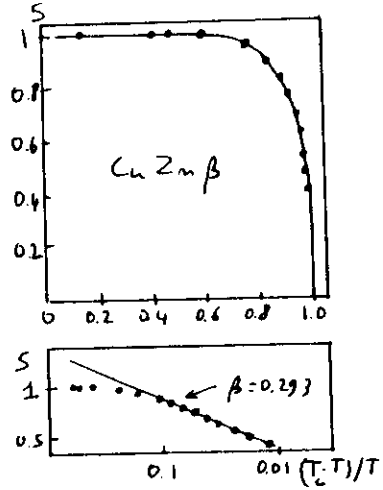

The critical scattering (divergence of the diffuse scattering close to T_c) gives also the correct temperature dependence at $\vec{Q} = \vec{\tau}_{100}$: it varies as $(1 - T_c/T)^{-\gamma}$, $\gamma = 1.24 \pm 0.015$ [28] ($\gamma = 1$ for mean-field model, see Clapp and Moss formula § IV).

Neutron scattering allows the study of phase transitions at very high temperature. In the Mo_2C system, where the Carbon atoms occupy half of the octahedral sites of the hcp metal lattice, a change of order was detected at 1300 °C and the order-disorder transition at 1950 °C [29]. At such high temperatures, a multidetector system is necessary to have short measuring times and avoid oxidation, changes of composition, etc.....

(c) Study of Debye-Waller factor by energy-dispersive X-ray diffraction

The precise determination of Debye-Waller factor necessitates to measure far in the reciprocal space. The energy dispersive X-ray diffraction method, which measures at fixed angle the diffraction from an incident white beam, can give precise results for relative variations.

In the considered study [30], single crystals NbC_{1-x} were placed with the <110> orientation, and the (h h 0) Bragg peaks recorded from h = 2 to 14, using the white spectrum of W.

The measurements were made up to $|q| = 30\ Å^{-1}$ ($E = 1.4$ to 60 keV, $\lambda = 0.20$ to $1.8\ Å$), at several temperatures and compositions. They allowed to separate the thermal vibration amplitudes and the static displacements ($|u_{Nb}| = 0.125 \pm 0.005\ Å$).

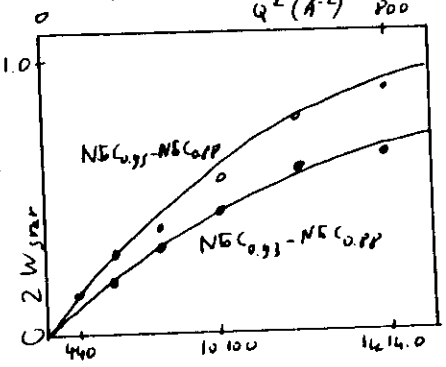

The static Debye-Waller factor deviates at large Q from the usual $\ln W \propto -Q^2$ formula, and follows the law proposed by KAIROGLOZ (see § II.2.c). (Counting time ≥ 1 hour for single crystal)

(d) Radiation induced disorder in A-15 superconductors

Large depressions of the critical temperature are observed when irradiating A15 compounds with fast (> 1 MeV) neutrons: for example, for Nb_3Al, T_c is decreased from 18.4 K to less than 1.4 K for a fluence $1.4\ 10^{19}\ n/cm^2$ [31] at 140 °K. Neutron diffraction studies showed a reduction of the LRO parameter S from 0.88 to 0.72 when T_c decreases from 18.4 to 9.6 K : the interpretation is a rate of depression of 2.2 K per % Nb sites occupied by Al atoms [31]. An expansion of the lattice parameter is also observed (5.183 → 5.200 Å).

Similar studies on V_3Si show also the importance of irradiation-induced static mean square displacements ($3 \cdot 10^{-2}$ Å for Si, $8 \cdot 10^{-2}$ Å for V, the latter obtained from channeling experiments) [32]

(e) Charge density maps

They are obtained by Fourier transform of the X-ray intensity diffracted by a single-crystal, and inform on the bonding. High-quality measurements have to be performed, and the thermal and static Debye-Waller effects corrected, as well as extinction. This was measured for example for TiC and TiN [33], and compared with charge densities from LAPW band calculations [34]. The agreement is good. In TiC, the charge distribution shows maxima in the <100> directions, indicating that the $3d\sigma_g$ orbitals (responsible for the Ti-C covalent bonding) are more occupied than the $3dt_{2g}$ (which point towards <110> and are responsible of Ti-Ti bonding). Charge transfer from Ti to metalloid (C or N) is confirmed (partial ionic bonding), but the amount depends on the model used to define the charge transfer (Mulliken partitioning, i.e. ionic-like orbitals $\Rightarrow$ 2 e^- charge transfer, versus spatial partitioning $\Rightarrow$ 0.5 e^-).

(f) Residual stresses.

X-ray diffraction is an important technique for non-destructive measurement of residual stresses (induced by surface working, forming, casting, welding, oxidation, etc...).

Two effects are generally observed:

- a broadening of the lines, which has been discussed in § II.1.6; it is due to non-uniform strains inside the coherent diffracting domains, due for example to dislocations or antigrain boundaries; one may obtain the mean square values of the associated strains, $\langle \varepsilon_n^2 \rangle^{1/2}$ on a length na ⊥ to the diffracting planes; of course, the ε_n are not independant;

for cold-worked samples, they are found to have practically a gaussian distribution, and follow the law $\langle \varepsilon_n^2 \rangle^{1/2} \simeq |n|^{\alpha} \langle \varepsilon_1^2 \rangle^{1/2}$ with $\alpha \simeq -0.5$ ($\langle \varepsilon_1^2 \rangle^{1/2}$ rms microstrain between cells).

- a shift of the lines, due to long-range stresses, these change the interplanar spacing d_{hkl}, and in a polycrystal, this will be dependent on the orientation of the plane (hkl) relative to the stress. This change of d_{hkl} can be measured by the change of the diffracting angle 2θ, when rotating the sample relatively to the incident beam; the stresses are obtained from the strains using linear isotropic elasticity. Generally, it is assumed that the principal stress σ_1 and σ_2 lie in the surface, and that $\sigma_3 = 0$. In the simplest case:

$$\sigma_\varphi = \sigma_1 \cos^2\varphi + \sigma_2 \sin^2\varphi = \frac{E}{1+\nu} \frac{1}{\sin^2\psi} \frac{d_{\varphi,\psi} - d_\perp}{d_\perp}$$

(E = Young modulus, ν = Poisson ratio), and measurements for different ψ and φ (see figure) lead to the stress tensor.

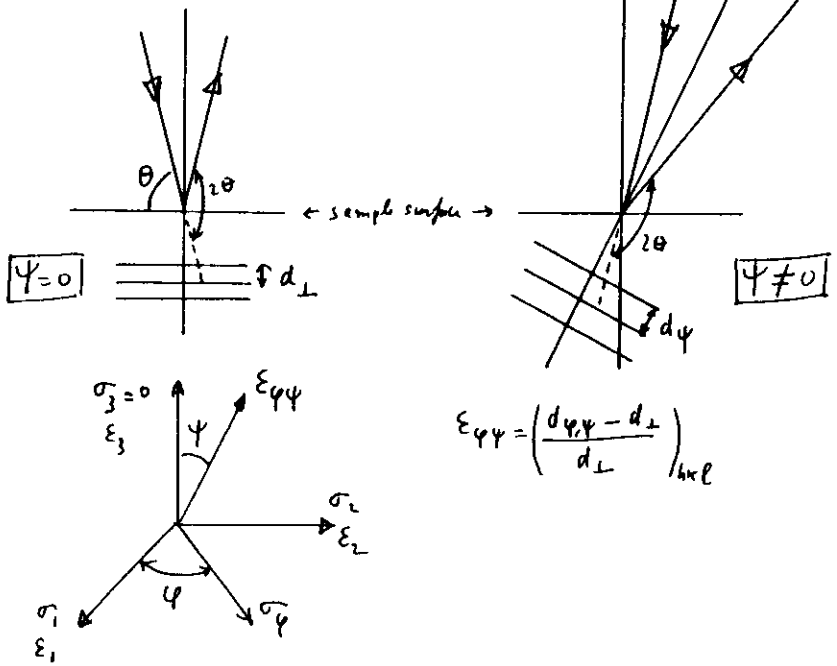

Detailed experimental procedures are found in the review article by JAMES and COHEN [35]

At particular useful application is stress profile measurements after mechanical surface treatments: shot peening induces compressive stress, which reduce crack propagation rates.

The stresses in each phase can be studied.

A single measurement at two ψ angles (0 and 45° for example) gives often an order of magnitude of the stress for control purpose (following its evolution after thermal treatments for example).

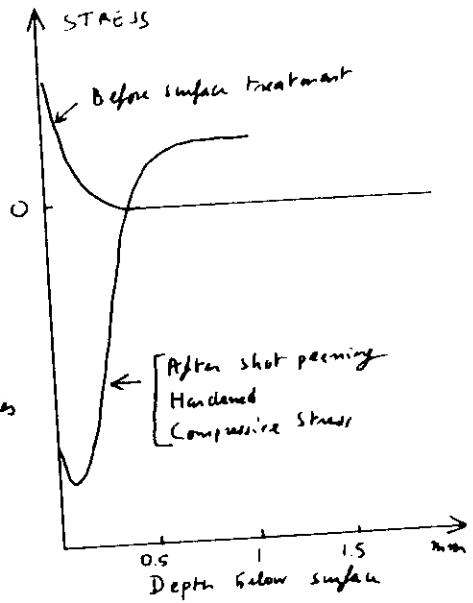

⑨ Use of glancing incidence X-ray diffraction for the study of implanted surfaces or thin films

The penetrating depth p of an X-ray beam incident on a surface with an angle α decreases rapidly when α goes below α_c, the critical angle of total reflexion. For iron, and Cu Kα ($\lambda = 1.54$ Å), $p \simeq 20$ Å for $\alpha < \alpha_c \simeq 0.2°$, $p \simeq 230$ Å for $\alpha = 0.5°$, 600 Å for $\alpha = 1°$ [36]

This shows the interest of realizing an X-ray diffractometer with low and adjustable glancing angle α.

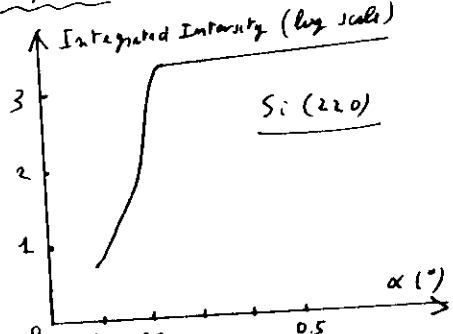

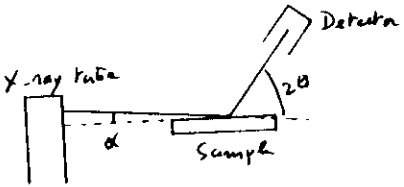

Such device have been realized: the divergence of the incident beam must be $\lesssim 0.02°$ and the surface of the sample polished.

Studies on austenitic steels allowed to observe a 100 Å thick martensitic layer formed during mechanical polishing; after electrochemical polishing (which eliminated this layer), and nitrogen implantation, the formation of nitrides was observed: (γ N in the $p < 100$ Å layer, and several other nitrides (ε and ζ - Fe_2N, Ni_3N, ...) for $100 < p < 1000$ Å [37]

⑩ Textures [38, 39]

Preferred grain orientation occurs in polycrystalline alloys, in particular after rolling or pilgering (deformation textures) or recrystallization (annealing textures). For a rolled sheet, a texture is qualitatively characterized by $(hkl)[uvw]$, where (hkl) is the lattice plane // rolling plane and $[uvw]$ the lattice direction // rolling direction. Mixed textures occur often.

Textures can be determined from X-ray or neutron diffraction, by the $(h'k'l')$ pole figures: one measure the integrated intensity of a Bragg peak $(h'k'l')$ for all orientations of the sample. A pole figure is obtained as follows:

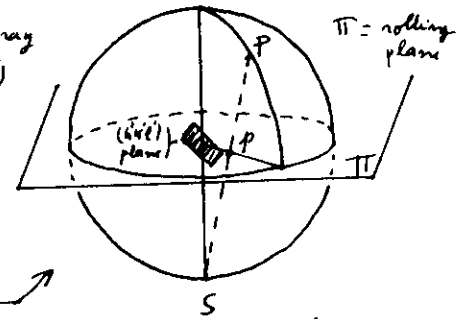

Π is the rolling plane (plane of the sheet); imagine all grains at the center of the sphere and plot the intersection $\mathbf{P}$ of the normals to $(h'k'l')$ with the sphere; trace the equi-intensity contours and make a stereographic projection on Π ($P \to p$).

Four $(h'k'l')$ pole figures for large grain pure Al annealing texture are shown on next page: several pole figures are necessary to determine the $(hkl)[uvw]$ set, in the present case $(100)\langle 001 \rangle$

Experimentally, the diffractometer is 4-circle. With X-rays, the center of the pole figure is explored by reflexion, the external part by transmission. Neutrons allow to average the texture on large volumes (≈ 1 cm³), X-rays to look at texture gradients.

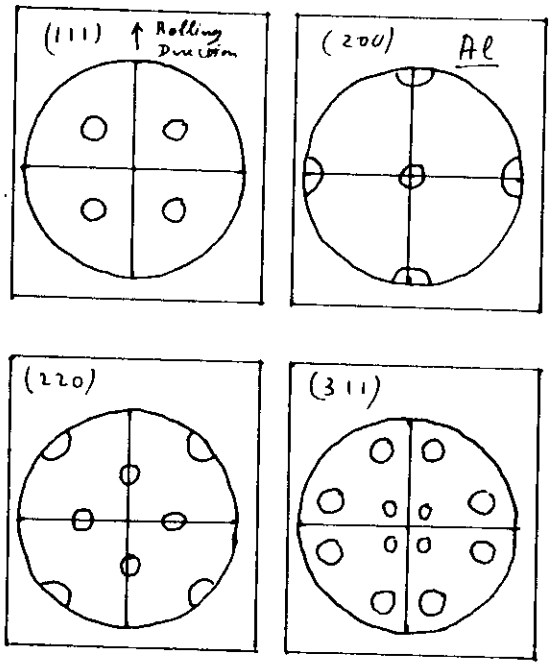

The quantitative texture is defined by an orientation distribution function $F(\vec{g})$ giving the distribution of grain orientations in $\vec{g}$ direction. The numerical determination of $F(\vec{g})$ from a set of direct pole figures has been the object of many developments.

⑤ Kinetics

The development of linear multichip textures allows kinetic diffraction experiments at the scale of the minute. The figure shows the isothermal time dependence of average ordered domain size deduced from (½ ½ ½) superlattice reflexion linewidth in $Ti_{1-x}C_x$ quenched from the disordered state to 735°C.

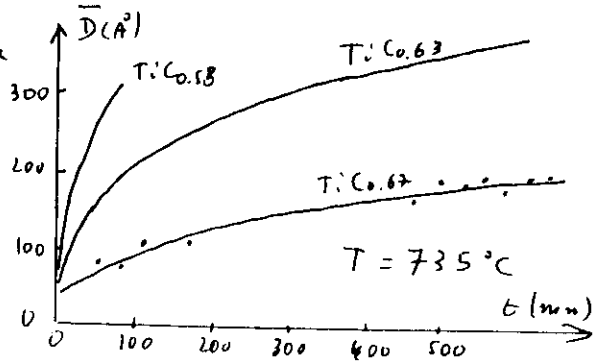

From a set of experiments at several temperatures, $\bar{D}^3 - \bar{D}_0^3 \simeq Ct$ (justified theoretically if there is a disordered film between ordered domains), an Arrhenius plot $\ln C = f(1/T)$ allows to obtain the carbon migration enthalpy 3.7 eV (trace experiments have to be made above 1500 °C) [40]

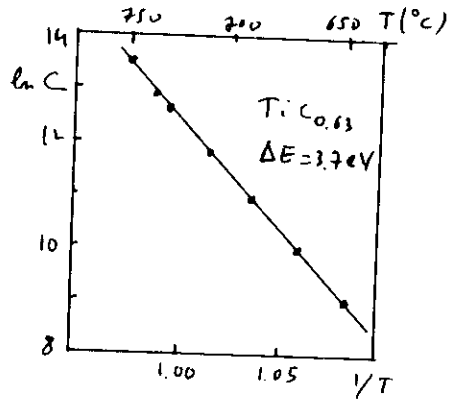

⑥ Modulated structures

Modulated structures characterized by a composition or displacement wave of wavelength $\vec{q_0}$ give rise to satellites at $\pm n\vec{q_0}$ around each Bragg reflexion in the reciprocal space [41, 42].

Disorder → order transformations are often accompanied by a loss of symmetry in the ordered state, giving splitting of Bragg reflexions (i.e. ordered CuAu is quadratic, (200) splits but not (111)). The distortions can be very small and only observed on single crystals with high resolution X-ray diffractometers; complications arise from the coexistence of different axial domains in a single crystal (i.e. for CuAu, $\vec{c}$ can take the three (100) orientations); this brings also strains (because of the distortion).

REFERENCES

[1] A. GUINIER, "X-ray Diffraction", Freeman, San Francisco (1963)

[2] G.E. BACON, "Neutron Diffraction", Clarendon Press, Oxford (1975)

[3] L.H. SCHWARTZ, J.B. COHEN, "Diffraction from Materials", Academic Press, New-York (1977)

[4] B.D. CULLITY, "Elements of X-ray Diffraction", Addison-Wesley, Reading, U.S.A. (1956)

[5] A. GUINIER, G. FOURNET, "Small-Angle Scattering of X-rays", Wiley, New-York (1955).

[6] M.A. KRIVOGLAZ, "Theory of X-ray and Thermal Neutron Scattering by Real Crystals", Plenum, New-York (1969).

[7] C.S. BARRETT, T.B. MASSALSKI, "Structure of Metals", Pergamon Press, Oxford (1980)

[8] "Neutron Scattering", ed. G. KOSTORZ, "Treatise on Materials Science and Technology" n°15, Academic Press, New-York (1979)

[9] "Local Atomic Arrangements Studied by X-ray Diffraction", ed. J.B. COHEN and J.E. HILLIARD, Gordon and Breach, New-York (1966).

[10] "Utilisation des faisceaux de neutrons en métallurgie" (in French), ed. J. JOFFRIN, Commissariat à l'Energie Atomique (DPhG), F-91191 CEN Saclay, France (1985)

[11] C.H. de NOVION, "Diffusion diffuse de rayons X et de neutrons", in "L'Ordre et le Désordre dans la Matière", Les Editions de Physique, Orsay, France (1984) (47 pp.).

[12] W. SCHMATZ, "X-ray and neutron scattering studies in disordered crystals", in "Treatise on Materials Science and Technology" n°2, ed. H. HERMAN, Academic Press, New-York (1973) p. 105.

[13] G. KOSTORZ, "X-ray and Neutron Scattering", in "Physical Metallurgy", 3rd edition, eds. R.W. CAHN and P. HAASEN, Elsevier, New-York (1983) pp 793-849.

[14] B.E. WARREN, "X-ray Diffraction", Addison-Wesley, Reading (1969).

[15] G.H. LANDER, D.L. PRICE, Physics Today (January 1985) pp 38-45.

[16] ILL Report, "Neutron Beam Facilities Available for Users", Grenoble, Institut Laue-Langevin (1986).

[17] H.G. HAUBOLD, J. Appl Crystallogr. 8 (1975) 175.

[18] "Synchrotron Radiation, Techniques and Applications", ed. C. KUNZ, Topics in Current Physics, Springer, Berlin (1979).

[19] H.M. RIETVELD, J. Appl. Crystallogr. 2 (1969) 65.

[20] K. TAKEMURA, K. SYASSEN, in "Solid State Physics under Pressure", ed. S. MINOMURA, Terra Scientific Publ. Comp. (1985) pp. 127-133

[21] M.J. GHUEZAIEL, Note CEA-N-2454, CEA-Saclay (1985)

[22] R.O. SIMMONS, R.W. BALLUFFI, Phys. Rev. 117 (1960) 52.

[23] T. ADLER, C.R. HOUSKA, J. Appl. Phys 50 (1979) 3282 and 3288

[24] C.R. HOUSKA, Treatise on Mat. Science and Technology 19A (1980) 63.

[25] Yu. A. IZYUMOV, R.P. OZEROV, "Magnetic Neutron Diffraction", Plenum Press, New-York (1970)

[26] W. TROST, K. DIETERT, K. MAIER, B. SEEBER, in Springer Proceedings in Physics n°10, Springer-Verlag (Berlin, 1986) p. 219

[27] O. RATHMANN, J. ALS-NIELSEN, Phys. Rev. B9 (1974) 3921.

[28] J. ALS-NIELSEN in "Phase Transitions and Critical Phenomena", ed. C. Domb and M.S. Green, Academic Press, London (1976) pp. 87.

[29] T. EPICIER, J. DUBOIS et al, to appear in Acta Metall. (1987)

[30] T.H. METZGER, J. PEISL, R. KAUFMANN, J. Phys. F: Metal Phys. 13 (1983) 1103

[31] A.R. SWEEDLER, D.E. COX, Phys. Rev. B 12 (1975) 147

[32] D.E. COX, J.A. TARVIN, Phys. Rev. B 18 (1978) 22

[33] A. DUNAND, H.D. FLACK, K. YVON, Phys. Rev. B 31 (1985) 2299

[34] P. BLAHA, J. REDINGER, K. SCHWARZ, Phys. Rev. B 31 (1985) 2316

[35] M.R. JAMES, J.B. COHEN, Treatise on Mat. Science and Technology, 19 A, Academic Press, New-York (1980) p. 1.

[36] M. BRUNEL, F. de BERGEVIN, Acta Cryst. A 42 (1986) 299.

[37] Y. BRNAUD, M. BRUNEL, et al, Applied Surface Science 26 (1986) 12

[38] "Textures in Research and Practice", J. GREWEN and G. WASSERMAN edit, Springer-Verlag, Berlin (1969)

[39] P. DERVIN in ref [10] p. 471

[40] V. HOISY-MAURICE, N. LORENZELLI, C.H. de NOUVION, P. CONVERT Acta Met. 30 (1982) 1769

[41] "Modulated Structures", AIP Conf. Proc. n°53, American Institute of Physics, New-York (1979)

[42] J.P. POUGET, in "Solid State Phase Transformations in Metals and Alloys", Les Editions de Physique, Orsay (France) (1980) p. 253.